Automatic detection of asphalt pavement raveling using image texture based feature extraction and stochastic gradient descent logistic regression

Nhat-Duc Hoang

Faculty of Civil Engineering, Institute of Research and Development, Duy Tan University, R.809 – No.03 Quang Trung, Da Nang 550000, Viet Nam

ABSTRACT

Raveling is one of the critical and pervasive modes of failure observed in asphalt pavement road. Automatic detection of raveling based on image samples is a challenging task due to the complex texture of asphalt pavement. This study constructs and investigates the capability of an image processing based approach for raveling recognition. Image texture based features extracted from statistical properties of color channels and the Gray-Level Co-Occurrence Matrix are employed as input variables to characterize the state of pavement. The Stochastic Gradient Descent Logistic Regression (SGD-LR) is used to classify image samples into two categories of non-raveling and raveling based on a set of extracted features. A SGD-LR based raveling detection program has been developed in Visual C# .NET to facilitate its implementation. Experimental outcome shows that the newly constructed approach can attain a good predictive performance with a classification accuracy rate of roughly 88%. Therefore, this approach can be a helpful tool to assist transportation authorities in the task of surveying asphalt pavement condition.

1. Introduction

Asphalt pavement is apparently the most common type of road surface [1,2]. The serviceability of this structure does not only affect the daily lives of people but is also strongly correlated with regional economic growth [3]. Therefore, ensuring the quality of asphalt road surface during serviceability time by early detection of road distresses and by performing timely maintenance activities is a crucial task of transportation agencies. It is because previous studies pointed out that poor maintenance can bring about significant increase in life cycle cost [4].

Due to the rapid expansion of the sheer length of road network coupled by the accelerated deterioration caused by extensive vehicle operation and inclement weather conditions, transportation agencies in many countries concurrently need to address the question: how to maintain road networks to ensure their serviceability and extend their life span with a constrained financial source [5]. Establishing pavement management systems is one of the most effective ways to provide an answer to the above challenging question. Nevertheless, the successful implementation of pavement management systems requires a large amount of data related to road network inventory, pavement inspection, and surface quality assessment/analysis.

With the advancement of image processing technology, the labor-intensive method of manual pavement inspection is replaced fully or partly by automated systems [6]. Recently, acquiring digital images of asphalt pavements from cameras mounted on vehicles can be a means for reducing hazardous working condition [7–11]. Moreover, semi-autonomous pavement distress detections and measurements can be achieved by the utilization of computer vision techniques. Therefore, extensive research works have been carried out to construct various systems capable of automatically recognizing different type of pavement distresses including cracks [12–17], patches [2,18,19], potholes [19–24], segregation [25], and raveling [4]. In recent years, various deep learning and image processing based models have been successfully employed in detecting defects of road surface and structural elements [17,26–31]. While cracks are line-based pavement defects which can be detected via edge detection algorithms, area-based detects such as patch and raveling can be recognized by analyzing pavement texture [2,4]. A review work done by Coenen and Golroo [5] pointed out that there is a critical need to focus additional research on pavement distress detection related to micro-texture analysis.

In addition, porous asphalt is often employed as the topmost layer within which large size stones constitute the road surface [32]. This type of layer has an advantage of allowing rain water to drain quickly; it also can help to decrease the noise disturbance caused by vehicles running on the road. However, one major drawback of porous asphalt is its susceptibility to raveling. Raveling (see Fig. 1) on asphalt pavement generally refers to a loss of aggregates from the asphalt matrix due to

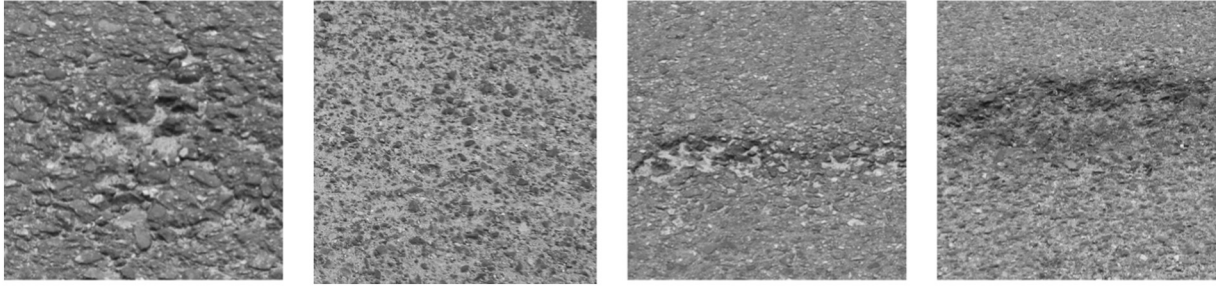*E-mail addresses:* hoangnhatduc@dtu.edu.vn, hoangnhatduc@duytan.edu.vn.

Fig. 1. Asphalt pavement raveling.

the friction between vehicle tires and asphalt layers [33]. In fact, raveling is one of the critical and pervasive modes of failure observed in asphalt pavement road [4,34]. This type of distress does not only reduce the ride convenience due to increase in pavement roughness but also brings about frequent road maintenance [4]. Tsai and Wang [34] pointed out that raveling may also cause severe traffic accidents due to hydroplaning. Therefore, timely detection of asphalt raveling area is a practicing need of transportation agencies in the task of periodic pavement survey.

Based on the existing literature, pavement raveling has not received as much attentions of the research community as other forms of pavement distress such as cracks and potholes. Considering the widely accepted negative effects of raveling on pavement quality, this study proposes an image processing based approach for asphalt pavement raveling detection. The rest of the paper is organized as follows: The second section reviews the related works, followed by the section of research methodology. The next section presents the newly constructed system used for pavement raveling detection, followed by the fifth section which reports experimental results. The final section contains several concluding remarks of this study.

2. Related works

Due to the importance of automatic pavement condition assessment, various studies have dedicated to developing method to recognize pavement raveling as well as other area-based pavement distress. Ong et al. [35] explored the utilization of objective laser measurements for characterizing pavement texture employed for raveling detection; this information was then analyzed within a network-level pavement management system. Mathavan et al. [33] relied on an image processing procedure that combines the visual information obtained from both 2-D and 3-D range images; a texture descriptor using Laws' texture energy measure is used in conjunction with Gabor filters and other digital signal processing techniques to recognize road section subject to raveling.

Tsai and Wang [34] introduced an asphalt pavement raveling recognition system; this system relied on 3D laser technology and macro-texture analysis; the extracted texture-based features were then employed as input factors for Random Forest models in the task of raveling classification. Radopoulou and Brilakis [20] relied on the semantic texton forests (STFs) algorithm as a supervised classifier to recognize different types of cracks (longitudinal and transverse), patches, and potholes. Hadjidemetriou et al. [2] proposed a pavement patch detection model which is based on Support Vector Machine; features extracted from image samples includes local intensity histogram, discrete cosine transform, and Gray-Level Co-Occurrence Matrix.

Massahi et al. [4] collected pavement data related to raveling using low-cost smartphone and based on the collected visual information, raveling pavement areas could be distinguished from intact pavement areas. Tong et al. [36] employed Convolutional Neural Network (CNN) for analyzing asphalt pavement surface texture; a convolutional neural network (CNN) is employed to calculate the mean texture depth (MTD);

accordingly, the trained CNN-based model is able to provide assessment of the surface texture statistics of highways. Aparna et al. [37] recently utilizes CNN and thermal imaging to analyze pavement texture for potholes detection; this study confirms the feasibility of thermal imaging application in pothole detection field.

Based on the literature review, it can be seen that image processing and machine learning can provide effective solutions for detecting area-based pavement distresses. Thus, the new approach proposed in this study relies on texture analysis to characterize the features of raveling pavement and intact pavement. The statistical information of image color is used in conjunction with properties derived from the Gray-Level Co-Occurrence Matrix. Accordingly, numerical features extracted from image texture are employed by the Logistic Regression to categorize image samples into raveling and non-raveling labels. In addition, the Stochastic Gradient Descent is employed as the training algorithm of the Logistic Regression model. This integrated system is then constructed in Visual C# .NET to ease its implementation.

3. Research methodology

3.1. Texture characterization using statistical properties of image colors

Because raveling belongs to the category of area-based defects, the texture of image regions can be used as features to separate areas subject to raveling from intact ones. Raveling and no-raveling pavement areas can express different properties related to appearance due to their dissimilarity in color, roughness, and texture homogeneity. Accordingly, the statistical properties of three color channels (red, green, and blue) of an image sample can be computed and used as predictors.

Let I be a variable that presents the gray levels of an image sample under analysis. The first-order histogram $P(I)$ is computed according to the following equation [38]:

$$P_c(I) = \frac{N_{I,c}}{W \times H} \tag{1}$$

where c represents one of the three color channels. $N_{I,c}$ denotes number of pixels with intensity value I of the channel c. H and W are the two variables representing the height and width of an image sample. Hence, $H \times W$ = the total number of pixels containing in an image sample.

Based on such definition, the mean of color value is calculated in the following manner:

$$\mu_c = \sum_{i=0}^{NL-1} I_{i,c} \times P_c(I) \tag{2}$$

where $NL = 256$ is the number of discrete intensity values since image samples are 8-bit.

The standard deviation of color in an image region can be obtained via the following formula:

$$\sigma_c = \sqrt{\sum_{i=0}^{NL-1} (I_{i,c} - \mu_c)^2 \times P_c(I)} \tag{3}$$

Besides the mean and the standard deviation, the Skewness and Kurtosis of color are also widely employed; their values can be calculated by the Eqs. (4) and (5) below:

$$\delta_c = \frac{\sum_{i=0}^{NL-1} (I_{i,c} - \mu_c)^3 \times P_c(I)}{\sigma_c^3} \tag{4}$$

$$\eta_c = \frac{\sum_{i=0}^{NL-1} (I_{i,c} - \mu_c)^4 \times P_c(I)}{\sigma_c^4} \tag{5}$$

Furthermore, the entropy and range of color of each pixel are computed using the Eqs. (6) and (7), respectively:

$$\rho_c = -\sum_{i=0}^{NL-1} P_c(I) \times \log_2(P_c(I)) \tag{6}$$

$$\Delta_c = Max(I_c) - Min(I_c) \tag{7}$$

3.2. Texture analysis using Gray-Level Co-Occurrence Matrix

Besides the aforementioned statistical color properties, the Gray-Level Co-Occurrence Matrix (GLCM) is a widely employed method for texture discrimination [39]. GLCM, first proposed in Haralick et al. [40], relies on the repeated occurrence of some gray-level patterns existing in the texture [2,41,42]. The gray-level configurations may vary acutely according to pixel distance in fine textures; these in coarse textures may vary in a slower manner. Since raveling and no-raveling pavement sections apparently have different fineness, using GLCM can potentially help to discriminate raveling pavement areas from no-raveling ones.

Let $\delta = (r, \theta)$ represent a vector in the polar coordinates of an image sample. For each of such vector, it is able to calculate the joint probability of the pairs of gray levels that occur at the two locations separated by the relationship $\delta = (r, \theta)$ [43]. The joint probability is summarized in a GLCM P_δ within which $P_\delta(i,j)$ denotes the probability of the two gray levels of i and j occurring at the relationship δ. It is noted after the construction of $P_\delta(i,j)$, this matrix is often normalized by the following equation:

$$P_\delta^N(i,j) = \frac{P_\delta(i,j)}{S_P} \tag{8}$$

where $P_\delta^N(i,j)$ is the normalized GLCM and S_P = the total number of pixels in the image.

Since computing P_δ with all possible values of r and θ requires a prohibitive amount of computational expense, Haralick et al. [40] recommended to calculate four GLCM with r = 1 and θ = 0°, 45°, 90°, and 135°. Based on these four GLCM, the properties of angular second moment (AM), contrast (CO), correlation (CR), and entropy (ET) can be extracted and used for texture discrimination. The formulas used for computing AM, CO, CR, and ET are described in the following equations [40,43]:

$$AM = \sum_{i=1}^{N_g} \sum_{j=1}^{N_g} P_\delta^N(i,j)^2 \tag{9}$$

where N_g = 256 denotes the number of gray level values.

$$CO = \sum_{k=0}^{N_g-1} k^2 \sum_{\substack{i=1 \\ |i-j|=k}}^{N_g} \sum_{j=1}^{N_g} P_\delta^N(i,j) \tag{10}$$

$$CR = \frac{\sum_{i=1}^{N_g} \sum_{j=1}^{N_g} i \times j \times P_\delta^N(i,j) - \mu_X \mu_Y}{\sigma_X \sigma_Y} \tag{11}$$

where μ_X, μ_Y, σ_X and σ_Y denote the means and standard deviations of the

marginal distribution associated with $P_\delta^N(i,j)$ [40]. These four quantities are computed as follows:

$$\mu_X = \sum_{i=1}^{N_g} i \sum_{j=1}^{N_g} P_\sigma^N(i,j) \tag{12}$$

$$\mu_Y = \sum_{j=1}^{N_g} j \sum_{i=1}^{N_g} P_\sigma^N(i,j) \tag{13}$$

$$\sigma_X = \sum_{i=1}^{N_g} (i - \mu_X)^2 \sum_{j=1}^{N_g} P_\sigma^N(i,j) \tag{14}$$

$$\sigma_Y = \sum_{j=1}^{N_g} (j - \mu_Y)^2 \sum_{i=1}^{N_g} P_\sigma^N(i,j) \tag{15}$$

$$ET = -\sum_{i=1}^{N_g} \sum_{j=1}^{N_g} P_\delta^N(i,j) \log(P_\delta^N(i,j)) \tag{16}$$

3.3. The collection of pavement image samples

Since the Logistic Regression is a supervised machine learning algorithm, a data set consisting of 1000 pavement image samples with the ground truth label has been collected to construct the Logistic Regression based classification model. Herein, the numbers of image samples in the two categories of non-raveling and raveling are both 500. The digital images have been collected during field trips of pavement survey in Danang city (Vietnam). The employed camera is the 18-megapixel resolution Canon EOS M10. The images were manually taken by human inspectors. The camera is positioned at a distance of about 1 m above the road surface. All images were taken in cloudy weather condition (from 4 pm to 6 pm) to maintain relatively similar lighting condition. The original image size is 5184 × 2912 pixels and 170 images have been collected during field trips of pavement survey.

Image samples of the two categories of non-raveling (label = 0) and raveling (label = 1) has been prepared for analysis. To expedite the speed of the feature extraction process, the size of image sample has been fixed to be 100 × 100 pixels. It is noted that the image samples used to train the machine learning model are created by cropping the original image. All image regions with raveling have been sampled in a non-overlapping manner. The areas of intact pavement have been randomly sampled. In addition, irregular areas (cracks, shadow, patches, stains, and traffic marks) are intentionally included in the category of non-raveling. Moreover, before being cropped, the size original images have been reduced to 50%. The illustration of the image sampling process is provided in Fig. 2a. The collected image samples are demonstrated in Fig. 2b. It is worth noticing that the ground truth label of each image sample is determine by human inspectors. Furthermore, the class of non-raveling includes samples of intact pavement, cracks, stains, and traffic marks to ensure the diversity of the image set.

3.4. Stochastic gradient descent logistic regression

The problem of interest is to establish a classification model to separate samples belonging to two possible categories: non-raveling (negative class) and raveling (positive class). Hence, it is suitable to apply the Logistic Regression model to tackle this pattern classification task [44]. The selection of the Logistic Regression is due to its straightforward implementation and successful applications in various engineering fields [45–51].

It is noted that the outcome (y) of the model is taken as $y = 1$ when the pavement image sample is subject to raveling and $y = 0$ when no raveling is observed.

Given an input feature $x_i = x_{i1}, x_{i2}, \ldots, x_{iD}$ where D is the number of the features used for classification and $\theta = \theta_0, \theta_1, \theta_2, \ldots, \theta_D$ denoting
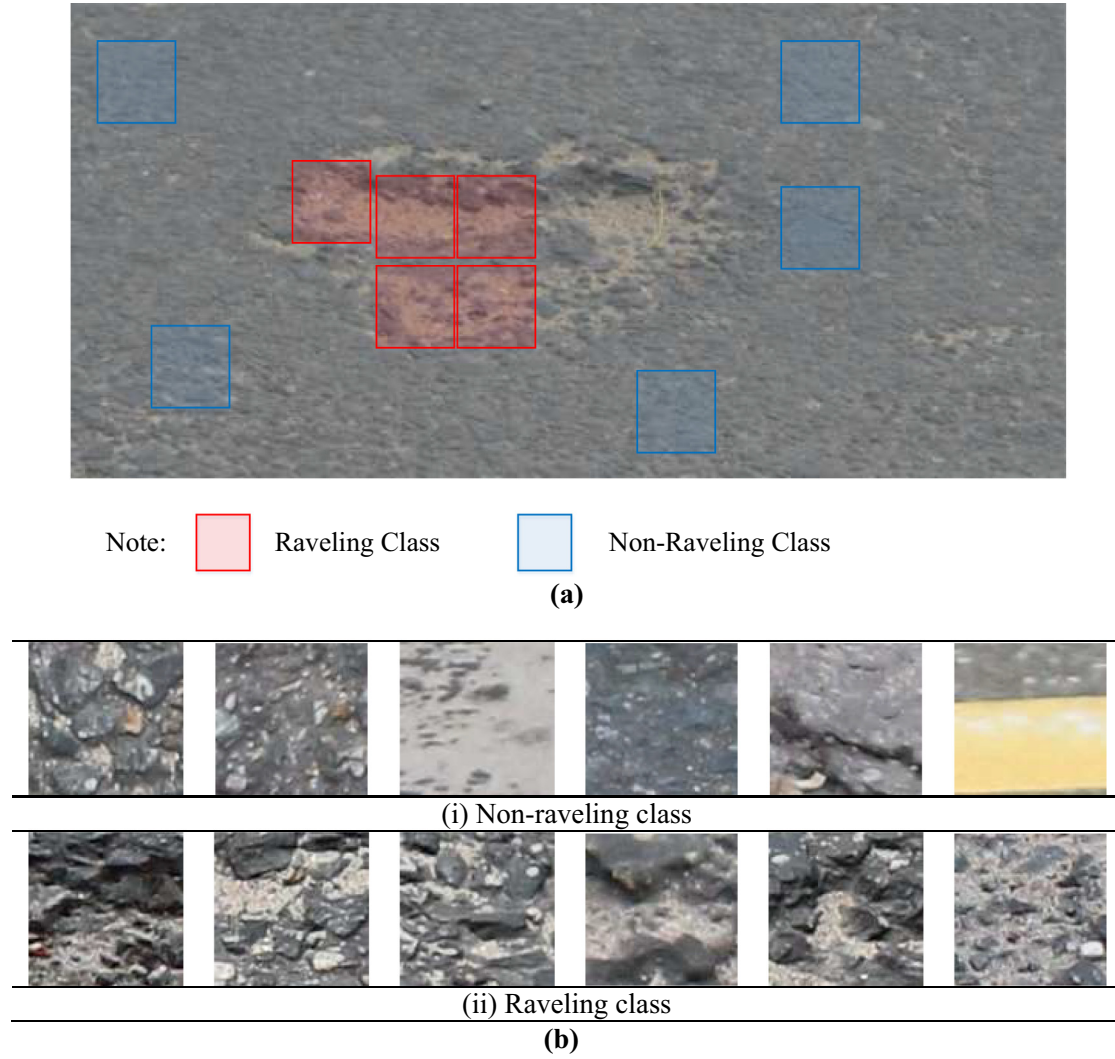
Fig. 2. The collected image samples: (a) Illustrations of the image sampling process and (b) Image samples of the non-raveling and raveling classes.

the Logistic Regression model parameters, the quantity $h_\theta(x_i)$ is used to express the probability of the positive class output of raveling. $h_\theta(x_i)$ is computed as follows [52]:

$$h_\theta(x_i) = h_\theta(x_{i1}, x_{i2}, ..., x_{iD}) = \frac{1}{1 + \exp(-\eta_i)} = \frac{1}{1 + \exp(-\theta^T x_i)} \quad (17)$$

where $\eta_i = \theta_0 + \theta_1 x_{i1} + \theta_2 x_{i2} + ... + \theta_D x_{iD} = \theta^T x_i$.

It is noted that $g(\eta_i) = \frac{1}{1 + \exp(-\eta_i)}$ is called the logistic function or the sigmoid function and its derivative is given as follows [53]:

$$g'(\eta_i) = g(\eta_i) \times (1 - g(\eta_i)) \quad (18)$$

The probabilities of the raveling ($y = 1$) and non-raveling ($y = 0$) classes are expressed as follows:

$$P(y_i = 1 \mid x_i, \theta) = h_\theta(x_i) \quad (19)$$

$$P(y_i = 0 \mid x_i, \theta) = 1 - h_\theta(x_i) \quad (20)$$

Thus, the output probability can be expressed compactly as follows [53]:

$$P(y_i \mid x_i, \theta) = (h_\theta(x_i))^{y_i} (1 - h_\theta(x_i))^{1-y_i} \quad (21)$$

Accordingly, the likelihood of the parameters can be written as follows [53]:

$$L(\theta) = \prod_{i=1}^{M} (h_\theta(x_i))^{y_i} (1 - h_\theta(x_i))^{1-y_i} \quad (22)$$

where M denotes the number of data samples.

To find the optimal model parameter θ, it is required to maximize the following log likelihood function:

$$l(\theta) = \log(L(\theta)) = \sum_{i=1}^{M} y_i \log\left(h_\theta(x_i)\right) + (1 - y_i)\left(1 - \log(h_\theta(x_i))\right) \quad (23)$$

The model parameter θ can be optimized via the Stochastic Gradient Descent (SGD) algorithm [54]. The procedure of the SGD is illustrated by a flowchart in Fig. 3. It is noted that the SGD algorithm requires the preparation of the training dataset with ground truth labels assigned to each data instance. In this flowchart, *MaxEpoch* denotes the maximum number of epochs and *ep* is the current training epoch. α represents the learning rate parameter. *M* is the number of data instances and *i* denotes the index of a data instance. Notably, the *k*th element of the model parameter θ_k is updated via the following equation:

$$\theta_k = \theta_k + \alpha \frac{\partial l(\theta_k)}{\partial(\theta_k)} \quad (24)$$

where $\frac{\partial l(\theta_k)}{\partial(\theta_k)}$ can be obtained as follows:

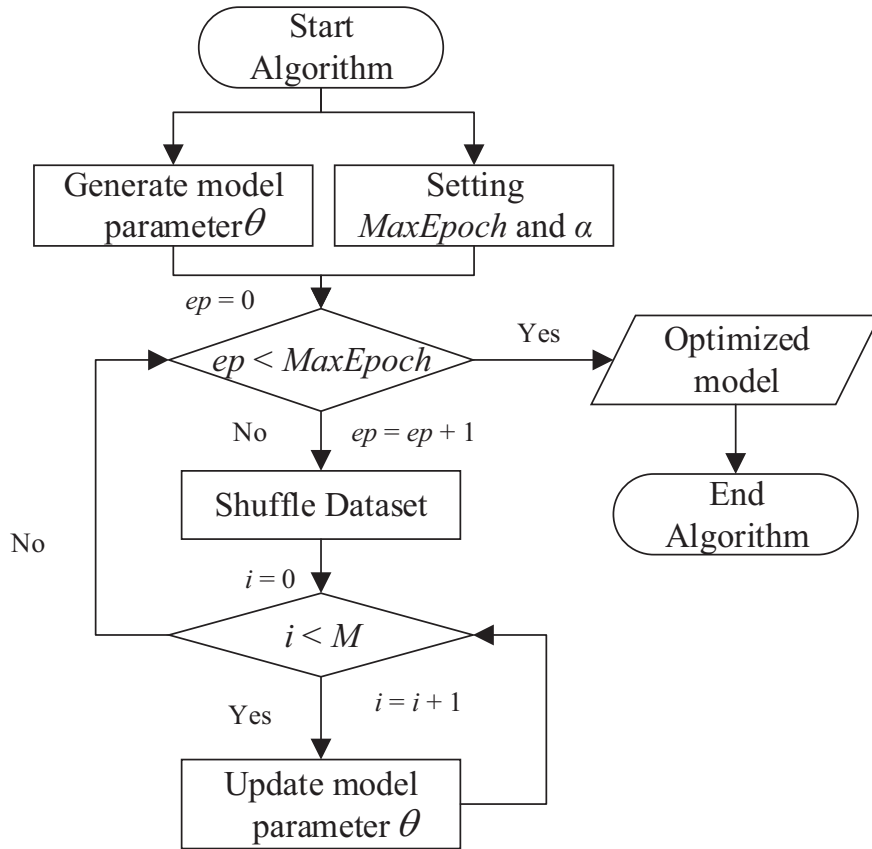$$\frac{\partial l(\theta_k)}{\partial(\theta_k)} = (y_i - h_\theta(x_i))x_{i,k} \quad (25)$$

Fig. 3. The Stochastic Gradient Descent (SGD) algorithm.

Therefore, the update rule used to determine the optimal model parameter θ is given as follows:

$$\theta_k = \theta_k + \alpha (y_i - h_\theta(x_i)) x_{i,k} \tag{26}$$

where $x_{i,\,0} = 1$ with all i.

4. The proposed approach for asphalt pavement raveling detection

The proposed model used for automatic asphalt pavement raveling detection is a hybridization of image processing and machine learning approaches. Image processing techniques including color property analysis and GLCM are utilized to extract useful features from the image samples. In addition, the SGD-LR is used in the data classification step to detect image samples containing raveling. The proposed model has been developed in Visual C# .NET (Framework 4.6.1) (see Fig. 4) and compiled to ease its implementation. The SGD-LR program is run on the ASUS FX705GE - EW165T (Core i7 8750H, 8GB Ram, 256GB solid-state drive); the graphics processing unit is NVIDIA GTX 1050Ti 4GB. In Fig. 4, it is noted that CAR denotes Classification Accuracy Rate.

In the step of feature extraction, the statistical properties of image color, including three channels of red, green, and blue, are computed. For each color channel, six statistical measurements of mean, standard deviation, skewness, kurtosis, entropy, and range are calculated according to the equation presented in the second section of the paper. Hence, the total number of input features extracted from the aforementioned statistical properties of image color a sample is 18. They are listed as follows:

- Mean of the three color channels of red, green, and blue (F1, F2, and F3)
- Standard deviation of the three color channels of red, green, and blue (F4, F5, and F6)
- Skewness of the three color channels of red, green, and blue (F7, F8, and F9)
- Kurtosis of the three color channels of red, green, and blue (F10, F11, and F12)
- Entropy of the three color channels of red, green, and blue (F13, F14, and F15)
- Range of the three color channels of red, green, and blue (F16, F17, and F18)

Moreover, the total number of features extracted from the constructed GLCM of each image sample is 16; they include the following variables:

- The angular second moment (F19), contrast (F20), correlation (F21), and entropy (F22) of GLCM with $r = 1$ and $\theta = 0°$
- The angular second moment (F23), contrast (F24), correlation (F25), and entropy (F26) of GLCM with $r = 1$ and $\theta = 45°$
- The angular second moment (F27), contrast (F28), correlation (F29), and entropy (F30) of GLCM with $r = 1$ and $\theta = 90°$
- The angular second moment (F31), contrast (F32), correlation (F33), and entropy (F34) of GLCM with $r = 1$ and $\theta = 135°$

It is noted that the feature extraction step finishes, a data set of 1000 samples is created for the data classification process. The extracted data set features 34 input variables and two class label of non-raveling (labeled as 0) and raveling (labeled as 1). The features extraction process of one negative (the first sample) and one positive sample (the second one) is demonstrated in Tables 1 and 2. It is also proper to note that the whole data set has been normalized by the Z-score equation which can help to enhance the training performance of machine learning models [55]. The equation of the Z-score data normalization is given as follows:
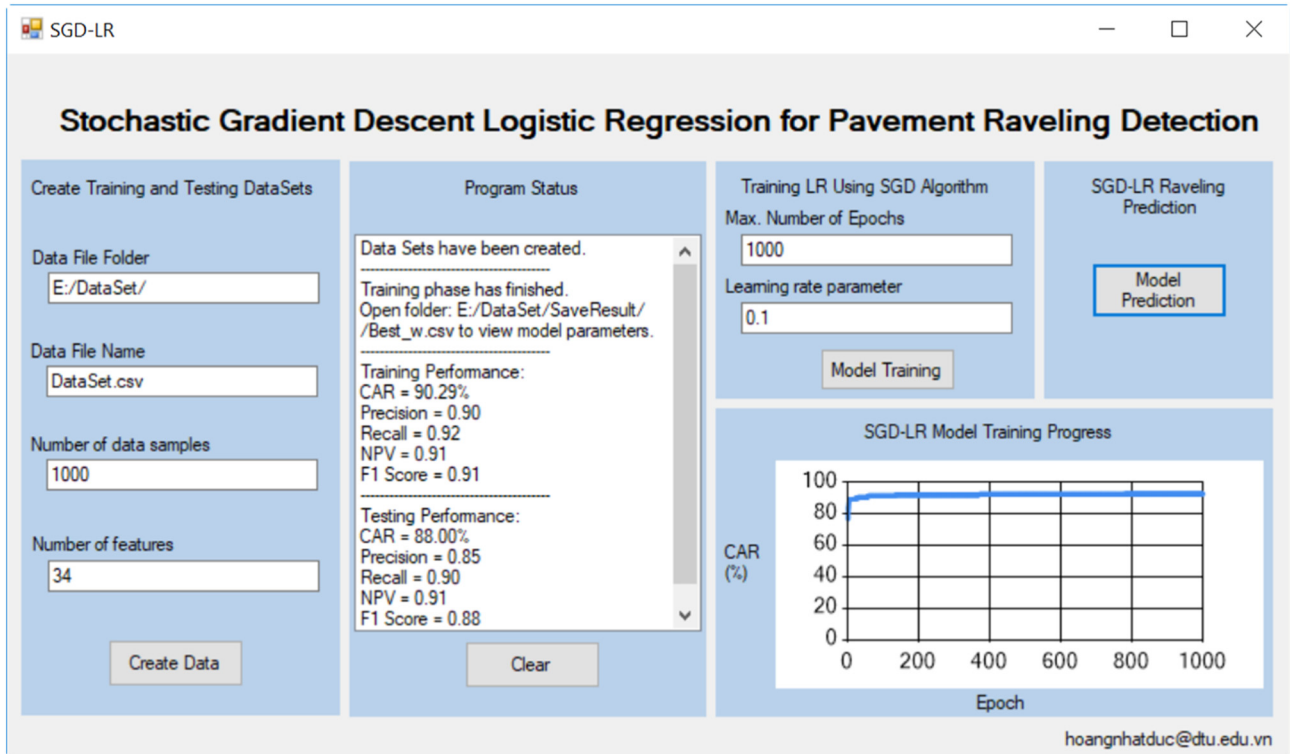
Fig. 4. Graphical user interface of the SGD-LR program used for pavement raveling detection.

$$X_{ZN} = \frac{X_o - m_X}{s_X} \qquad (27)$$

where X_o and X_{ZN} represent an original and a normalized input variable, respectively. m_X and s_X denote the mean and the standard deviation of the original input variable, respectively.

The newly created data set is then randomly divided into two sets of training (70%) and testing data (30%). The training set is employed to construct the SGD-LR model; the testing set is reserved for assessing the model generalization capability. In addition, to appraise the model performance, the following performance measurement metrics have been employed [56]:

$$\text{Classification Accuracy Rate:CAR} = \frac{TP + TN}{TP + TN + FP + FN} \times 100\% \qquad (28)$$

where TP, TN, FP, and FN are the true positive, true negative, false positive, and false negative values.

$$\text{Precision} = \frac{TP}{TP + FP} \qquad (29)$$

Table 2
Extracted GLCM features.

Image sample	Extracted GLCM feature			
	Angular second moment	Contrast	Correlation	Entropy
	0.0016	35.9579	0.0039	9.9948
	0.0010	110.0963	0.0032	10.6137
	0.0013	65.1318	0.0036	10.3085
	0.0011	74.5557	0.0036	10.4077
	0.0003	288.2543	0.0007	12.1841
	0.0002	665.7685	0.0006	12.4561
	0.0002	508.8808	0.0006	12.3785
	0.0002	715.9790	0.0005	12.4796

$$\text{NPV} = \frac{TN}{TN + FN} \qquad (30)$$

Table 1
Extracted color features.

Image sample	Extracted color feature					
	Mean	Std	Skewness	Kurtosis	Entropy	Range
	86.4005	15.6527	1.0727	5.5118	5.8933	132.0000
	91.6253	15.4635	1.0359	5.2349	5.8747	125.0000
	98.9229	15.2172	0.9207	4.9004	5.8728	129.0000
	115.8801	36.7558	0.1214	2.9208	7.2135	217.0000
	113.8447	36.8411	0.0872	2.9111	7.2237	220.0000
	113.5898	36.1354	0.0535	2.9659	7.1907	219.0000

Table 3
Demonstration of the training and testing data sets.

Data set	Data	F1	F2	F3	F4	F5	...	F30	F31	F32	F33	F34	Class
Training	1	173.52	173.92	173.61	14.14	14.70	...	9.83	0.0013	71.72	0.0040	10.24	0
	2	171.87	172.08	171.80	12.99	14.25	...	9.55	0.0015	52.55	0.0046	10.03	0
	3	165.24	165.32	164.86	20.52	21.20	...	10.08	0.0012	75.83	0.0021	10.51	0
	4	172.27	172.64	172.47	15.44	16.03	...	9.93	0.0012	75.94	0.0034	10.33	0
	5	166.62	167.15	166.99	18.48	19.14	...	10.10	0.0010	67.16	0.0026	10.58	0
	...	...	...	...	...	...	...	...	...	...	...	...	...
	696	127.76	127.06	125.80	22.96	22.74	...	11.25	0.0005	158.88	0.0017	11.43	1
	697	128.25	125.60	123.97	20.42	20.63	...	10.95	0.0006	152.81	0.0020	11.19	1
	698	125.15	122.15	120.17	21.07	21.26	...	11.09	0.0005	147.00	0.0019	11.28	1
	699	106.21	105.77	104.10	27.40	25.89	...	11.30	0.0005	184.33	0.0013	11.54	1
	700	120.23	118.85	115.96	30.73	29.25	...	11.51	0.0004	220.09	0.0010	11.73	1
Testing	1	122.49	122.99	123.29	34.91	33.77	...	11.95	0.0003	409.99	0.0007	12.17	0
	2	133.16	134.21	134.99	32.57	32.70	...	11.64	0.0004	337.16	0.0008	11.79	0
	3	121.38	122.13	123.75	30.07	29.68	...	11.80	0.0003	441.34	0.0009	12.00	0
	4	130.70	130.22	129.64	35.50	34.72	...	12.10	0.0003	473.28	0.0007	12.25	0
	5	131.95	132.80	133.15	30.11	30.16	...	11.80	0.0004	345.36	0.0009	11.86	0
	...	...	...	...	...	...	...	...	...	...	...	...	...
	296	132.37	129.08	124.75	24.38	22.94	...	11.37	0.0004	195.65	0.0015	11.52	1
	297	121.63	119.34	116.09	26.22	24.57	...	11.47	0.0004	197.88	0.0014	11.60	1
	298	129.11	126.25	122.61	26.06	25.10	...	11.41	0.0004	225.81	0.0013	11.56	1
	299	137.87	135.36	131.26	20.24	19.03	...	10.83	0.0007	133.05	0.0023	11.02	1
	300	119.15	117.86	116.21	23.63	22.25	...	11.35	0.0004	171.97	0.0017	11.50	1

$$\text{Recall} = \frac{TP}{TP + FN} \qquad (31)$$

$$\text{F1 Score} = \frac{2TP}{2TP + FP + FN} \qquad (32)$$

5. Experimental results

As mentioned in the previous section, the data set, which consists of 1000 samples and 34 input features, has been divided into training and testing subsets. The training and testing subsets contains 70% and 30% of the original collected data set, respectively. The first set is employed in the model construction phase; the second set is reserved for evaluating the model generalization capability when predicting raveling status in novel image samples. It is noted that in both training and testing data sets, the numbers of raveling and non-raveling samples are equal. Table 3 provides demonstrations of training and testing data sets.

Furthermore, because one time of model training and testing cannot well reveal the model generalization capability due to the randomness in data selection [57], this study has performed a random subsampling of the original data set. This random subsampling process contains 20 runs. In each run, 30% of the data is randomly drawn to form the testing set; the rest of the data is used for model training purpose. As can be seen from the training process of SGD-LR, it is required to select the parameters of learning rate and the maximum number of epochs. Based on several trial-and-error runs, the suitable values of these two parameters are found to be 0.1 and 1000, respectively.

With these hyper-parameters, the performance in terms of CAR of the SGD-LR is 88.12%. It is noted that the model performance indicator mentioned above is the average of result of CAR values obtained from the repeated subsampling data with 20 runs. In addition, the training progresses of the SGD-LR model are demonstrated in Fig. 5. The model structure of the SGD-LR model expressed in form of a weight vector is reported in Fig. 6. The first element of the weight vector is the bias. The other elements are weighting values associated with the 34 employed features extracted from image samples. Using the information provided in Fig. 6, the LR model used for raveling detection can be constructed instantly without the need of re-training process.

Moreover, the class probabilities of several image samples yielded by the SGD-LR model are demonstrated in Fig. 7. As can be seen from Fig. 7a, the model has successfully recognized a sound pavement surface based on texture of the image sample (the probability of the
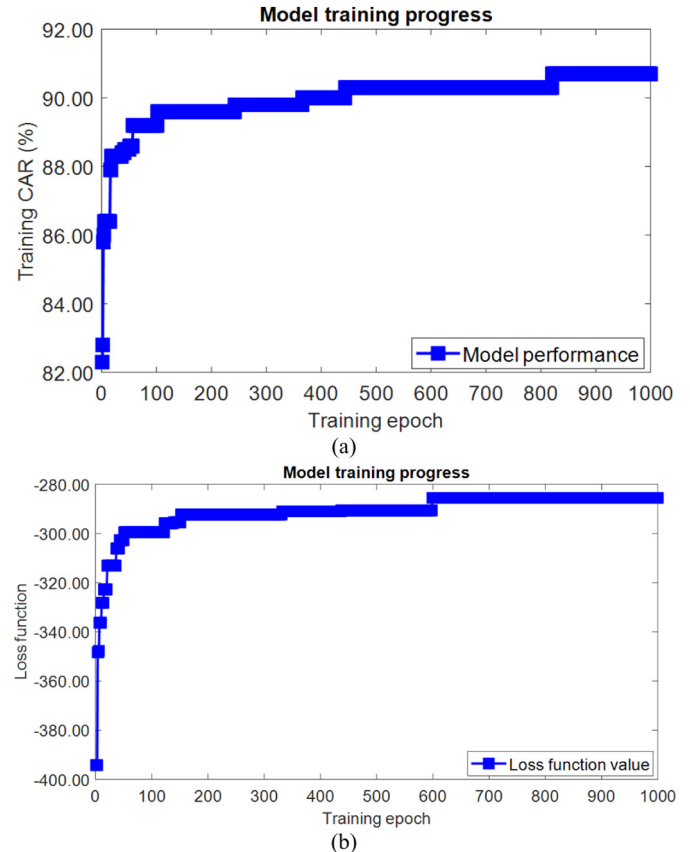

Fig. 5. Model training progress: (a) CAR and (b) Loss function.

negative class is 0.79). However, as can be seen in Fig. 7b, shadow has adversely affects the model accuracy because a non-raveling case has falsely classified as raveling. An example shown in Fig. 7c demonstrates that the model can perform well in the presence of cracks. In addition, the model correctly detects raveling samples (Fig. 7d and e) even when the image is affected by shadow (Fig. 7e).

To confirm the prediction capability of the employed SGD-LR used for pavement raveling detection, its performance has been compared to
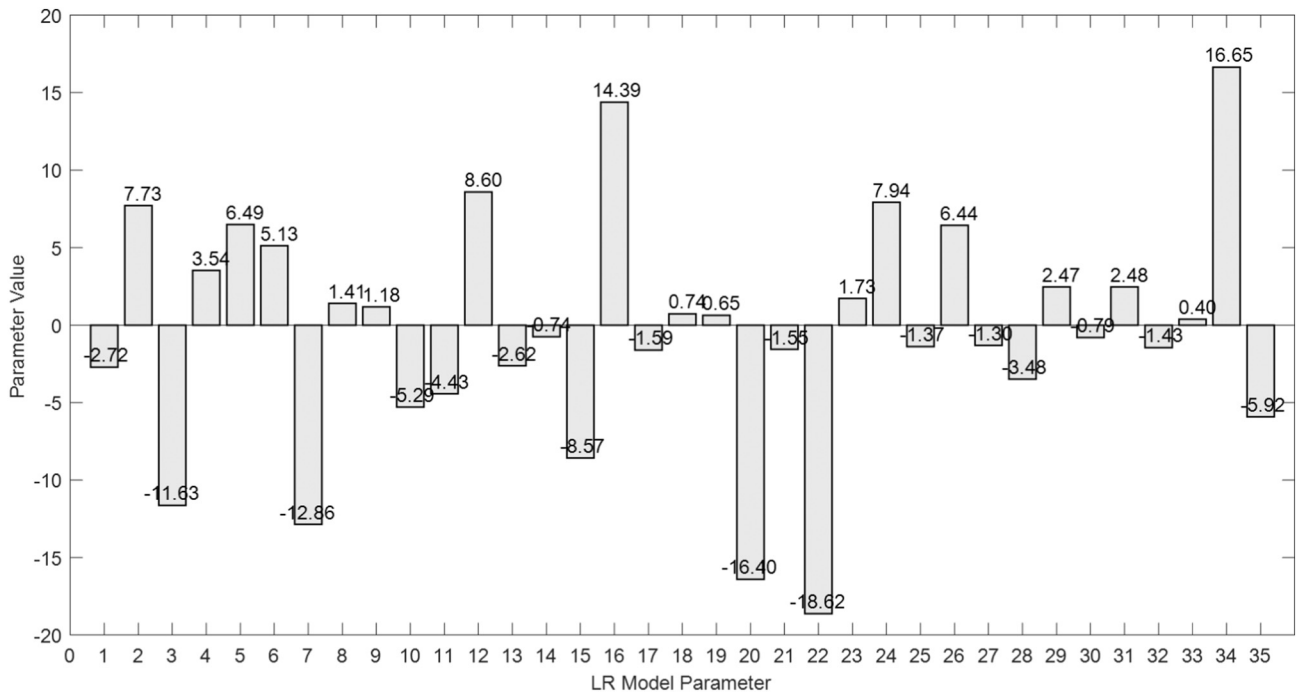
Fig. 6. Parameter of the SGD-LR found by the training process.

that of the Classification Tree (CTree) [58] and Convolution Neural Network (CNN) [59]. CTree, proposed by Breiman et al. [60], is a widely employed method for pattern classification [61,62]. This machine learning method is highly effective in discovering structural patterns in data and presenting the data in the form of a tree-like structure [63]. A CTree model is constructed by splitting subsets of the training dataset using all features to build two child nodes [64]. The most suitable feature is chosen via the Gini impurity function [65]. The CT algorithm aims at creating data subsets which are as homogeneous as possible for each class label. In addition, CNN is a machine learning approach that relies on deep learning framework [17]. Notably, the feature extraction phase is automatically performed by convolution layers.

The reason of this model selection is that the CTree model has been confirmed to be a capable method for solving complex data classification in recent research works [50,66–68]. Moreover, CNN has been proved to be an effective method for detecting pavement distress including cracks [69,70], potholes [37,71], and rutting [72]. However, the capability of CNN in detecting pavement raveling has not been investigated. In this study, the CTree model is implemented via the MATLAB Statistics and Machine Learning Toolbox [73]. To utilize a CTree, it is necessary to specify the parameter of minimum leaf size. Via several trial runs, the appropriate value of this parameter of the CTree model is found to be 8.

In addition, the CNN model (illustrated in Fig. 8) used for raveling detection in this study is trained via the MATLAB deep learning toolbox [74]; the Adam algorithm developed by Kingma and Ba [75] and the mini-batch mode have been employed to train the deep network model. Rectified Linear Units (ReLU) are utilized as activation functions. Based on experimental runs, the suitable configuration of the CNN is as follows: Input image size is 30×30 pixels. The number of convolution layers is 6. The detailed description of the convolution layers and pooling layers are shown in Table 4. In addition, a batch normalization layer is employed between convolutional layers and the ReLU. The batch normalization layer aims at normalizing each input data across a mini-batch [74]. Moreover, a fully connected layer is used between the last pooling layer and the softmax layer [74,76]. By experiments, the suitable mini-batch size is 200 and the maximum number of training

epochs is 5000.

The prediction results of the SGD-LR and the employed benchmark model are summarized in Table 5 which reports the mean, standard deviation (Std), and coefficient of variation (COV) [77] of the model performance. It is noted that a similar ratio of training to testing dataset is employed for SGD-LR, CTree, and CNN. The classification time periods of the SGD-LR and CTree models for one image sample are mostly determined by the feature extraction phase. The time period requires for extracting the aforementioned 34 features is about 8.41s. In addition, the CNN does not require the feature extraction process and only requires 0.0014s for classifying one image sample.

The prediction results of the employed model are graphically presented in Figs. 9 and 10. As can be observed from the experimental outcomes, the performance of SGD-LR (CAR = 88.12%, Precision = 0.85, Recal = 0.93, NPV = 0.92, and F1 score = 0.89) is better than that of CNN (CAR = 87.93%, Precision = 0.87, Recal = 0.89, NPV = 0.89, and F1 score = 0.88) and CTree (CAR = 84.45%, Precision = 0.84, Recal = 0.84, NPV = 0.86, and F1 score = 0.85). As can be seen from Table 1, the training performances of CTree (93%) and CNN (93.39%) are higher than that of SGD-LR (89.71%). Nevertheless, the testing outcome of SGD-LR (CAR = 88.12%) is significantly better than those of CTree (CAR = 84.45%) and CNN (CAR = 78.37%). These facts mean that both CTree and CNN models suffer from overfitting problem. Notably, since the testing performance of SGD-LR is relatively close to that of the training performance, it can be seen that this model has achieved a balance between model accuracy and complexity.

Moreover, the Wilcoxon signed-rank test [78] is employed in this section to confirm the statistical difference of each pair of raveling detection methods. This statistical test is a non-parametric method widely used for model comparison [57]. Herein, the significance level of the test is set to be 0.05. If the *p*-value of the Wilcoxon signed-rank test is lower than this threshold, it is able to conclude that the classification results obtained from the two raveling detection models are statistically different. Based on the CAR values obtained from the repeated data sampling with 20 runs, the Wilcoxon signed-rank confirms that the raveling detection outcome of the SGD-LR is statistically different than the that of the CTree with the *p*-values = 0.0002. However, the hypothesis test regarding the SGD-LR and CNN models yields the *p*-
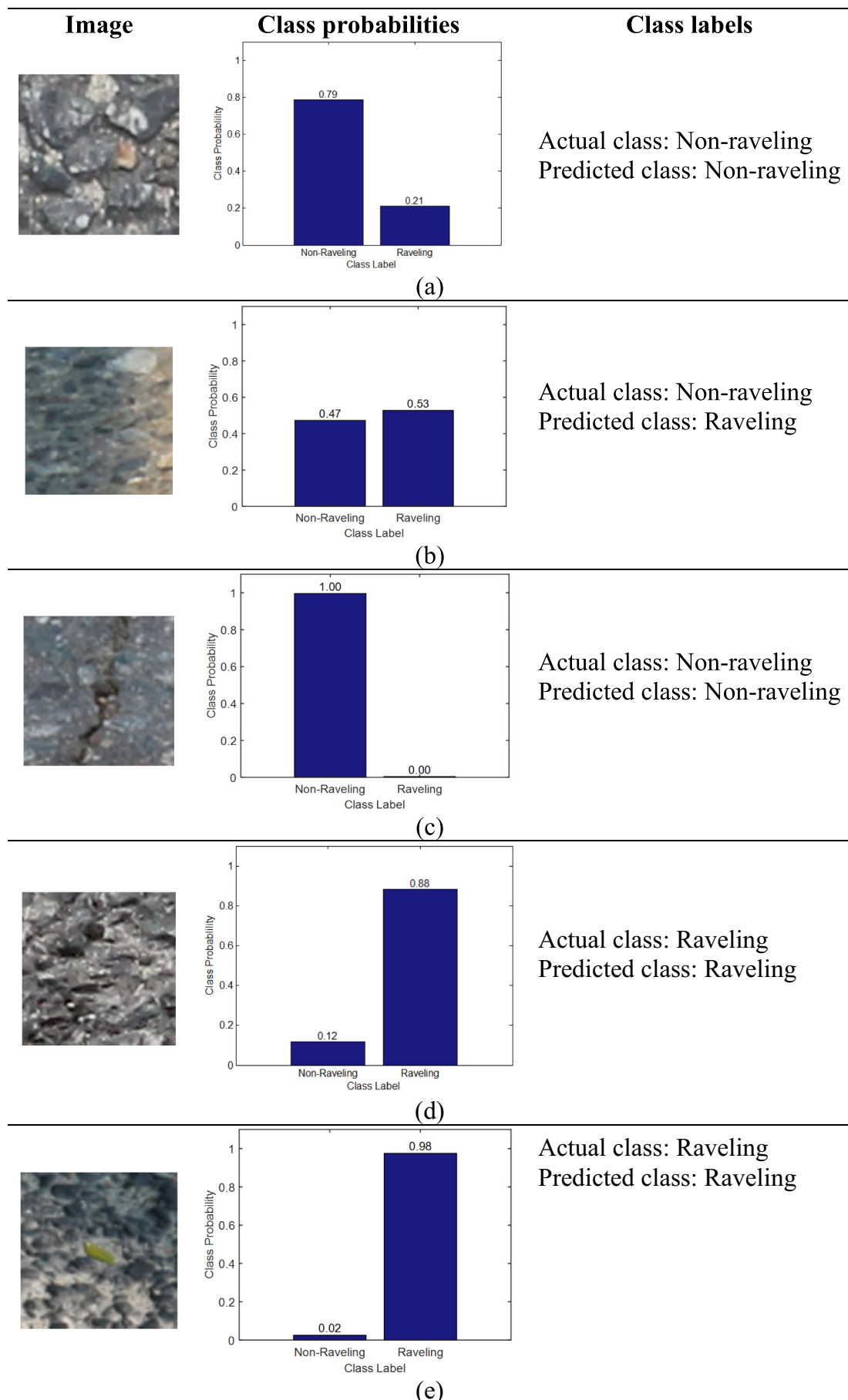
Image	Class probabilities	Class labels

(a) Actual class: Non-raveling / Predicted class: Non-raveling

(b) Actual class: Non-raveling / Predicted class: Raveling

(c) Actual class: Non-raveling / Predicted class: Non-raveling

(d) Actual class: Raveling / Predicted class: Raveling

(e) Actual class: Raveling / Predicted class: Raveling

Fig. 7. Illustrations of class probabilities of image samples predicted by the SGD-LR model.
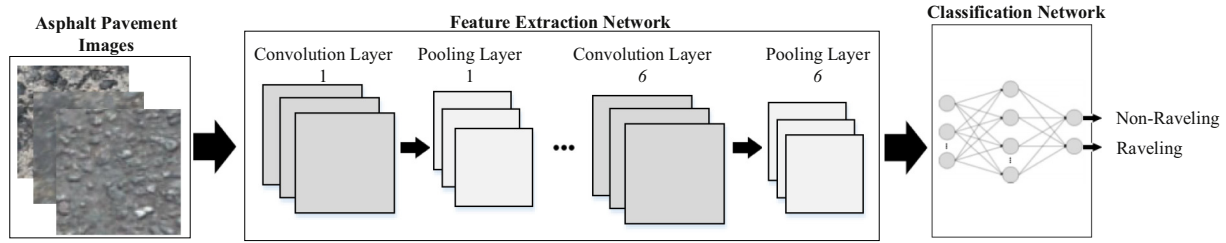
Fig. 8. Structure of the CNN model.

Table 4
Parameters of the CNN model.

CNN layers	Convolution layers		Pooling layers
	Filter number	Filter size	Filter size
1	49	2	2
2	49	2	2
3	36	2	2
4	36	2	2
5	25	2	2
6	25	2	2

Fig. 9. Prediction result comparison in terms of CAR, Precision, Recall, NPV, and F1 Score.

values = 0.9108. This fact indicates that the performance of the SGD-LR is comparable to that of the CNN. Nevertheless, since the CAR (88.12%), Recal (0.93), NPV (0.92), and F1 score (0.89) of the SGD-LR integrated with the employed image processing based feature extraction process is better than those of the CNN (with CAR = 87.93%, Recal = 0.89, NPV = 0.89, and F1 score = 0.88), it is able to conclude that the SGD-LR is a highly suitable method for the task of pavement raveling detection.

6. Conclusion

Raveling is a serious type of asphalt pavement distress. Therefore, recognizing this type of distress in a timely manner is a practical need of pavement management agencies. This study constructs an automated approach for asphalt pavement raveling detection that combines the advantages of image processing and machine learning methods. Image processing techniques have been used to extract useful features from asphalt pavement image samples to characterize the pavement
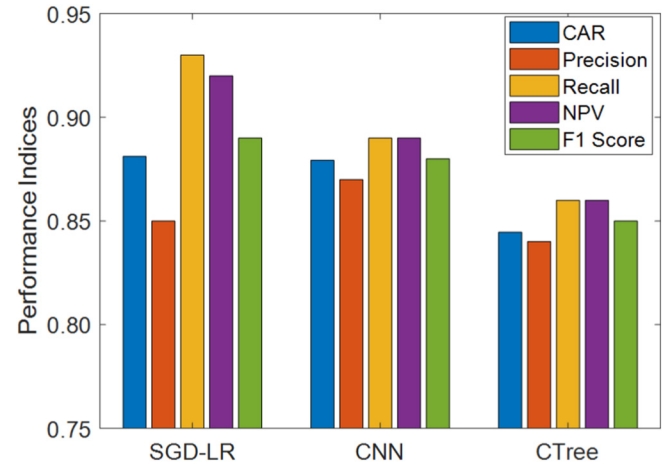
condition. In total, 34 features can be extracted using statistical properties of image color and the GLCM. Moreover, 1000 image samples have been collected to train and verify the employed machine learning approach of SGD-LR. Experimental results point out that the SGD-LR model can achieve a desired predictive performance with an average CAR = 88.12%. Moreover, a software program of the SGD-LR model has been developed to facilitate its implementation. Therefore, the newly constructed model can be a useful tool for transportation authorities to quickly assert the pavement condition.

Further extensions of the current research work include the

Table 5
Model performance comparison.

| Phase	Measurement indices	Models								
		SGD-LR			CTree			CNN		
		Mean	Std	COV	Mean	Std	COV	Mean	Std	COV
Training	CAR (%)	89.71	0.70	0.78	93.00	0.69	0.74	98.57	0.83	0.84
	TP	328.50	4.30	1.31	327.90	4.17	1.27	319.60	4.03	1.26
	TN	299.50	5.87	1.96	323.10	5.27	1.63	321.10	2.49	0.78
	FP	50.50	5.87	11.63	26.90	5.27	19.59	3.90	2.49	63.85
	FN	21.50	4.30	19.99	22.10	4.17	18.85	5.40	4.03	74.66
	Precision	0.87	0.01	1.48	0.92	0.01	1.45	0.99	0.01	0.77
	Recall	0.94	0.01	1.31	0.94	0.01	1.27	0.98	0.01	1.26
	NPV	0.93	0.01	1.23	0.94	0.01	1.17	0.98	0.01	1.23
	F1	0.90	0.01	0.70	0.93	0.01	0.72	0.99	0.01	0.86
Testing	CAR (%)	88.12	2.14	2.43	84.45	2.51	2.98	87.93	2.20	2.50
	TP	139.15	3.59	2.58	128.80	6.57	5.10	133.15	3.44	2.58
	TN	125.20	5.45	4.36	124.55	5.99	4.81	130.65	5.30	4.06
	FP	24.80	5.45	21.99	25.45	5.99	23.52	19.35	5.30	27.41
	FN	10.85	3.59	33.07	21.20	6.57	30.97	16.85	3.44	20.40
	Precision	0.85	0.03	3.30	0.84	0.03	3.67	0.87	0.03	3.44
	Recall	0.93	0.02	2.58	0.86	0.04	5.10	0.89	0.02	2.58
	NPV	0.92	0.02	2.67	0.86	0.04	4.20	0.89	0.02	2.36
	F1	0.89	0.02	2.22	0.85	0.03	3.11	0.88	0.02	2.39
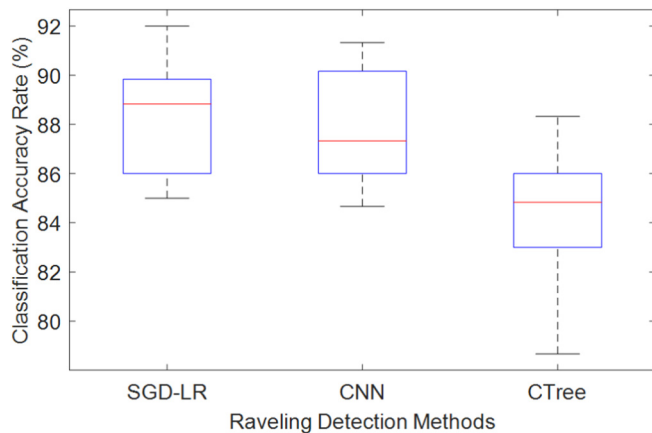
Fig. 10. Results of CAR obtained from the repeated subsampling process with 20 runs.

employment of other advanced algorithms for training logistic regression models to enhance its classification performance, expansion of collected set of image samples to improve the generalization of the current approach, utilization of advanced deep learning algorithms (e.g. AlexNet with transfer learning strategy [79,80]), and performing real-time process of pavement images. In addition, shadow existed on pavement surface may cause incorrect classifications; hence, shadow removal techniques can be utilized to improve the raveling detection outcome. Detecting raveling based on air photogrammetry and images from a static city camera can also be worth investigating research directions. In addition, the integration of the current SGD-LR based raveling detection with Geographic Information System mapping technology can significantly help local authorities in road network management.

Declaration of Competing Interest

The author confirms that there are no conflicts of interest regarding the publication of this paper.

Appendix A. Supplementary data

The supplementary file provides the dataset used in this study and the SGD-LR program used for raveling detection. The first 34 columns of the data are texture based features extracted from image samples. The last column is the ground truth label of the data instance with 0 = "Non-Raveling" and 1 = "Raveling". The dataset and the developed program can be accessed via: https://github.com/NhatDucHoang/SGD_LR_PaveRaveling.

References

[1] NAPA, Asphalt pavement industry survey on recycled materials and warm-mix asphalt usage, National Asphalt Pavement Association, https://www.asphaltpavement.org/PDFs/IS138/IS138-2017_RAP-RAS-WMA_Survey_Executive_Summary.pdf, (2017) , Accessed date: 11 March 2019.

[2] G.M. Hadjidemetriou, P.A. Vela, S.E. Christodoulou, Automated pavement patch detection and quantification using support vector machines, J. Comput. Civ. Eng. 32 (2018) 04017073, https://doi.org/10.1061/(ASCE)CP.1943-5487.0000724.

[3] E. Ivanová, J. Masárová, Importance of road infrastructure in the economic development and competitiveness, Econ. Manag. 18 (2013) 263–274, https://doi.org/10.5755/j01.em.18.2.4253.

[4] A. Massahi, H. Ali, F. Koohifar, M. Baqersad, and M. Mohammadafzali, "Investigation of pavement raveling performance using smartphone," International Journal of Pavement Research and Technology, vol. 11, pp. 553–563, 2018/11/01/ 2018, https://doi.org/10.1016/j.ijprt.2017.11.007.

[5] T.B.J. Coenen, A. Golroo, A review on automated pavement distress detection methods, Cogent Engineering 4 (09/05/2017), https://doi.org/10.1080/23311916.2017.1374822.

[6] H. Zakeri, F.M. Nejad, A. Fahimifar, Image based techniques for crack detection, classification and quantification in asphalt pavement: a review, Archives of

[7] Computational Methods in Engineering 24 (November 01 2017) 935–977, https://doi.org/10.1007/s11831-016-9194-z.

[7] Y. Pan, X. Zhang, G. Cervone, L. Yang, Detection of asphalt pavement potholes and cracks based on the unmanned aerial vehicle multispectral imagery, IEEE Journal of Selected Topics in Applied Earth Observations and Remote Sensing 11 (2018) 3701–3712, https://doi.org/10.1109/JSTARS.2018.2865528.

[8] G.M. Hadjidemetriou, S.E. Christodoulou, Vision- and entropy-based detection of distressed areas for integrated pavement condition assessment, J. Comput. Civ. Eng. 33 (2019) 04019020, https://doi.org/10.1061/(ASCE)CP.1943-5487.0000836.

[9] K. Doycheva, C. Koch, M. König, Computer Vision and Deep Learning for Real-time Pavement Distress Detection, Cham (2019), pp. 601–607.

[10] Z. Li, C. Cheng, M.-P. Kwan, X. Tong, S. Tian, Identifying asphalt pavement distress using UAV LiDAR point cloud data and random forest classification, ISPRS International Journal of Geo-Information 8 (2019) 39.

[11] L. Inzerillo, G. Di Mino, R. Roberts, Image-based 3D reconstruction using traditional and UAV datasets for analysis of road pavement distress, Autom. Constr. 96 (2018) 457–469 2018/12/01/ https://doi.org/10.1016/j.autcon.2018.10.010.

[12] N.-D. Hoang, Q.-L. Nguyen, V.-D. Tran, d, Autom. Constr. 94 (2018) 203–213 2018/10/01/ https://doi.org/10.1016/j.autcon.2018.07.008.

[13] A. Cubero-Fernandez, F.J. Rodriguez-Lozano, R. Villatoro, J. Olivares, J.M. Palomares, Efficient pavement crack detection and classification, EURASIP Journal on Image and Video Processing 2017 (2017) 39 2017/06/13 https://doi.org/10.1186/s13640-017-0187-0.

[14] S. Mokhtari, L. Wu, H.-B. Yun, Comparison of supervised classification techniques for vision-based pavement crack detection, Transportation Research Record: Journal of the Transportation Research Board 2595 (2016) 119–127, https://doi.org/10.3141/2595-13.

[15] K. Zhang, H.D. Cheng, B. Zhang, Unified approach to pavement crack and sealed crack detection using preclassification based on transfer learning, J. Comput. Civ. Eng. 32 (2018) 04018001, , https://doi.org/10.1061/(ASCE)CP.1943-5487.0000736.

[16] A. Zhang, K.C.P. Wang, B. Li, E. Yang, X. Dai, Y. Peng, et al., Automated pixel-level pavement crack detection on 3D asphalt surfaces using a deep-learning network, Computer-Aided Civil and Infrastructure Engineering 32 (2017) 805–819, https://doi.org/10.1111/mice.12297.

[17] Y.-J. Cha, W. Choi, O. Büyüköztürk, Deep learning-based crack damage detection using convolutional neural networks, Computer-Aided Civil and Infrastructure Engineering 32 (2017) 361–378, https://doi.org/10.1111/mice.12263.

[18] S.C. Radopoulou, I. Brilakis, Patch detection for pavement assessment, Autom. Constr. 53 (2015) 95–104 2015/05/01/ https://doi.org/10.1016/j.autcon.2015.03.010.

[19] P. Wang, Y. Hu, Y. Dai, M. Tian, Asphalt pavement pothole detection and segmentation based on wavelet energy field, Math. Probl. Eng. 2017 (2017) 13, https://doi.org/10.1155/2017/1604130.

[20] S.C. Radopoulou, I. Brilakis, Automated detection of multiple pavement defects, J. Comput. Civ. Eng. 31 (2017) 04016057, , https://doi.org/10.1061/(ASCE)CP.1943-5487.0000623.

[21] M.H. Yousaf, K. Azhar, F. Murtaza, F. Hussain, Visual analysis of asphalt pavement for detection and localization of potholes, Adv. Eng. Inform. 38 (2018) 527–537 2018/10/01/ https://doi.org/10.1016/j.aei.2018.09.002.

[22] N.-D. Hoang, An artificial intelligence method for asphalt pavement pothole detection using least squares support vector machine and neural network with steerable filter-based feature extraction, Advances in Civil Engineering (2018) 1–12, https://doi.org/10.1155/2018/7419058.

[23] S. Gothane, M.V. Sarode, V.M. Thakre, Prediction for Indian road network images dataset using feature extraction method, In Proc. of the First International Conference on Artificial Intelligence and Cognitive Computing, Singapore, 2019, pp. 125–138, , https://doi.org/10.1007/978-981-13-1580-0_12.

[24] E. Buza, A. Akagic, S. Omanovic, H. Hasic, Unsupervised method for detection of high severity distresses on asphalt pavements, 2017 IEEE 14th International Scientific Conference on Informatics, 2017, pp. 45–50, , https://doi.org/10.1109/INFORMATICS.2017.8327220.

[25] M. Baqersad, A. Hamedi, M. Mohammadafzali, H. Ali, Asphalt mixture segregation detection: digital image processing approach, Adv. Mater. Sci. Eng. 2017 (2017) 6, https://doi.org/10.1155/2017/9493408.

[26] S. Dorafshan, R.J. Thomas, M. Maguire, Comparison of deep convolutional neural networks and edge detectors for image-based crack detection in concrete, Constr. Build. Mater. 186 (2018) 1031–1045 2018/10/20/ https://doi.org/10.1016/j.conbuildmat.2018.08.011.

[27] F.C. Chen, M.R. Jahanshahi, NB-CNN: deep learning-based crack detection using convolutional neural network and Naive Bayes data fusion, IEEE Trans. Ind. Electron. 65 (2018) 4392–4400, https://doi.org/10.1109/TIE.2017.2764844.

[28] S. Dorafshan, R.J. Thomas, M. Maguire, Benchmarking image processing algorithms for unmanned aerial system-assisted crack detection in concrete structures, Infrastructures 4 (2019) 19, https://doi.org/10.3390/infrastructures4020019.

[29] S. Dorafshan, M. Maguire, W. Collins, Infrared thermography for weld inspection: feasibility and application, Infrastructures 3 (2018) 45.

[30] D.J. Atha, M.R. Jahanshahi, Evaluation of deep learning approaches based on convolutional neural networks for corrosion detection, Struct. Health Monit. 17 (2018) 1110–1128, https://doi.org/10.1177/1475921717737051.

[31] K. Gopalakrishnan, S.K. Khaitan, A. Choudhary, A. Agrawal, Deep Convolutional Neural Networks with transfer learning for computer vision-based data-driven pavement distress detection, Constr. Build. Mater. 157 (2017) 322–330 2017/12/30/ https://doi.org/10.1016/j.conbuildmat.2017.09.110.

[32] M. Miradi, Neural network models for analysis and prediction of raveling, IEEE Conference on Cybernetics and Intelligent Systems, 2004, 2004, pp. 1226–1231, ,

https://doi.org/10.1109/ICCIS.2004.1460766.

[33] S. Mathavan, M.M. Rahman, M. Stonecliffe-Jones, K. Kamal, Pavement raveling detection and measurement from synchronized intensity and range images, Transp. Res. Rec. 2457 (2014) 3–11, https://doi.org/10.3141/2457-01.

[34] Y. J. Tsai and Z. Wang, "Development of an asphalt pavement raveling detection algorithm using emerging 3D laser technology and macrotexture analysis," Final Report for NCHRP IDEA Project 163, Final Report for NCHRP IDEA ProjeTransportation Research Board, Washington, DC, http://www.trb.org/Main/Blurbs/173944.aspx (Last Access Date: 03/15/2019), 2015,

[35] G. P. Ong, W. Flora, A. S. Noureldin, and K. C. Sinha, "Statistical modeling of pavement raveling using texture measurements," In Proc. of the Transportation Research Board 87th Annual Meeting, Washington DC, United States, 2008-1-13 to 2008-1-17, https://trid.trb.org/view/847468 (Last Access Date: 03/15/2019), 2008,

[36] Z. Tong, J. Gao, A. Sha, L. Hu, S. Li, Convolutional neural network for asphalt pavement surface texture analysis, Computer-Aided Civil and Infrastructure Engineering 33 (2018) 1056–1072, https://doi.org/10.1111/mice.12406.

[37] Aparna, Y. Bhatia, R. Rai, V. Gupta, N. Aggarwal, A. Akula, Convolutional neural networks based potholes detection using thermal imaging, Journal of King Saud University - Computer and Information Sciences (2019), https://doi.org/10.1016/j.jksuci.2019.02.004 2019/02/05/.

[38] S. Theodoridis, K. Koutroumbas, Pattern Recognition, Printed in the United States of America Academic Press, 978-1-59749-272-0, 2009.

[39] R.M. Haralick, L.G. Shapiro, Computer and Robot Vision, Addison-Wesley Longman Publishing Co., Inc., Boston, MA, USA, 0201569434, 1992.

[40] R.M. Haralick, K. Shanmugam, I. Dinstein, Textural features for image classification, IEEE Transactions on Systems, Man, and Cybernetics SMC-3 (1973) 610–621, https://doi.org/10.1109/TSMC.1973.4309314.

[41] M. Sonka, V. Hlavac, and R. Boyle, Image Processing, Analysis, and Machine Vision: Cengage Learning, Printed in the United States of America, ISBN-10: 1-133-59360-7, 2013.

[42] Z. Zhang, F. Gao, B. Ma, Z. Zhang, Extraction of earth surface texture features from multispectral remote sensing data, Journal of Electrical and Computer Engineering 2018 (2018) 9, https://doi.org/10.1155/2018/9684629.

[43] F. Tomita, S. Tsuji, Computer Analysis of Visual Textures, Springer Science + Business Media, New York, 978-1-4612-8832-9, 1990, https://doi.org/10.1007/978-1-4613-1553-7.

[44] W.W. Piegorsch, Statistical Data Analytics: Foundations for Data Mining, Informatics, and Knowledge Discovery, John Wiley & Sons, Ltd, 978-1-118-61965-0, 2015.

[45] C. Polykretis, C. Chalkias, Comparison and evaluation of landslide susceptibility maps obtained from weight of evidence, logistic regression, and artificial neural network models, Nat. Hazards (April 09 2018), https://doi.org/10.1007/s11069-018-3299-7.

[46] B.T. Pham, D. Tien Bui, I. Prakash, Landslide susceptibility assessment using bagging ensemble based alternating decision trees, logistic regression and J48 decision trees methods: a comparative study, Geotech. Geol. Eng. 35 (December 01 2017) 2597–2611, https://doi.org/10.1007/s10706-017-0264-2.

[47] M. Andrejiova, A. Grincova, D. Marasova, Failure analysis of rubber composites under dynamic impact loading by logistic regression, Eng. Fail. Anal. 84 (2018) 311–319 2018/02/01/ https://doi.org/10.1016/j.engfailanal.2017.11.019.

[48] H. Lee, J.A. Chun, H.-H. Han, S. Kim, Prediction of frost occurrences using statistical modeling approaches, Adv. Meteorol. 2016 (2016) 9, https://doi.org/10.1155/2016/2075186.

[49] A.U. Haq, J.P. Li, M.H. Memon, S. Nazir, R. Sun, A hybrid intelligent system framework for the prediction of heart disease using machine learning algorithms, Mob. Inf. Syst. 2018 (2018) 21, https://doi.org/10.1155/2018/3860146.

[50] M. Chang, M. Maguire, Y. Sun, Stochastic modeling of bridge deterioration using classification tree and logistic regression, J. Infrastruct. Syst. 25 (2019) 04018041, , https://doi.org/10.1061/(ASCE)IS.1943-555X.0000466.

[51] K. Shaaban, D. Muley, D. Elnashar, Evaluating the effect of seasonal variations on walking behaviour in a hot weather country using logistic regression, Int. J. Urban Sci. 22 (2018) 382–391 2018/07/03 https://doi.org/10.1080/12265934.2017.1403363.

[52] A. Agresti, An Introduction to Categorical Data Analysis, John Wiley & Sons, Inc, Hoboken, NJ 07030, USA, 9781119405283, 2019.

[53] A. Ng, Lecture notes, Stanford University, http://cs229.stanford.edu/notes/cs229-notes1.pdf, (2018) , Accessed date: 13 December 2018.

[54] M. Gormley, Logistic Regression, https://www.cs.cmu.edu/~mgormley/courses/10701-f16/slides/lecture5.pdf, (2016) , Accessed date: 12 December 2018.

[55] D. Tien Bui, H.V. Le, N.-D. Hoang, GIS-based spatial prediction of tropical forest fire danger using a new hybrid machine learning method, Ecological Informatics 48 (2018) 104–116 2018/11/01/ https://doi.org/10.1016/j.ecoinf.2018.08.008.

[56] N.-D. Hoang, Q.-L. Nguyen, Metaheuristic optimized edge detection for recognition of concrete wall cracks: a comparative study on the performances of Roberts, Prewitt, Canny, and Sobel Algorithms, Advances in Civil Engineering 2018 (2018) 16, https://doi.org/10.1155/2018/7163580.

[57] N.-D. Hoang, D.T. Bui, Predicting earthquake-induced soil liquefaction based on a hybridization of kernel Fisher discriminant analysis and a least squares support vector machine: a multi-dataset study, Bull. Eng. Geol. Environ. 77 (February 01 2018) 191–204, https://doi.org/10.1007/s10064-016-0924-0.

[58] L. Breiman, J.H. Friedman, R.A. Olshen, C.J. Stone, Classification and Regression Trees, Wadsworth and Brooks, Montery, CA, USA, 0412048418, 1984.

[59] Y. LeCun, Y. Bengio, G. Hinton, Deep learning, Nature 521 (2015) 436–444 05/28/print https://doi.org/10.1038/nature14539.

[60] L. Breiman, J.H. Friedman, R.A. Olshen, C.J. Stone, Classification and Regression Trees, Wadsworth and Brooks, Montery, Calif, USA, 1984 ISBN-13: 978-0412048418.

[61] B.T. Pham, D. Tien Bui, I. Prakash, M.B. Dholakia, Rotation forest fuzzy rule-based classifier ensemble for spatial prediction of landslides using GIS, Nat. Hazards 83 (August 01 2016) 97–127, https://doi.org/10.1007/s11069-016-2304-2.

[62] W. Chen, X. Xie, J. Wang, B. Pradhan, H. Hong, D. T. Bui, et al., "A comparative study of logistic model tree, random forest, and classification and regression tree models for spatial prediction of landslide susceptibility," CATENA, vol. 151, pp. 147–160, 2017/04/01/ 2017, https://doi.org/10.1016/j.catena.2016.11.032.

[63] L. Roka, O. Maimon, Data Mining With Decision Trees: Theory and Applications, World Scientific Publishing Company, 978-981-277-171-1, 2008.

[64] M.S. Alkhasawneh, U.K. Ngah, L.T. Tay, N.A. Mat Isa, M.S. Al-Batah, Modeling and testing landslide hazard using decision tree, J. Appl. Math. 2014 (2014) 9, https://doi.org/10.1155/2014/929768.

[65] N.-D. Hoang, Q.-L. Nguyen, Automatic recognition of asphalt pavement cracks based on image processing and machine learning approaches: a comparative study on classifier performance, Math. Probl. Eng. 2018 (2018) 16, https://doi.org/10.1155/2018/6290498.

[66] K. Khosravi, B. T. Pham, K. Chapi, A. Shirzadi, H. Shahabi, I. Revhaug, et al., "A comparative assessment of decision trees algorithms for flash flood susceptibility modeling at Haraz watershed, northern Iran," Sci. Total Environ., vol. 627, pp. 744–755, 2018/06/15/ 2018, https://doi.org/10.1016/j.scitotenv.2018.01.266.

[67] H. Hong, J. Liu, D.T. Bui, B. Pradhan, T.D. Acharya, B.T. Pham, et al., Landslide susceptibility mapping using J48 Decision Tree with AdaBoost, Bagging and Rotation Forest ensembles in the Guangchang area (China), CATENA 163 (2018) 399–413 2018/04/01/ https://doi.org/10.1016/j.catena.2018.01.005.

[68] L.-J. Wang, M. Guo, K. Sawada, J. Lin, J. Zhang, A comparative study of landslide susceptibility maps using logistic regression, frequency ratio, decision tree, weights of evidence and artificial neural network, Geosci. J. 20 (February 01 2016) 117–136, https://doi.org/10.1007/s12303-015-0026-1.

[69] B. Li, K.C.P. Wang, A. Zhang, E. Yang, G. Wang, Automatic classification of pavement crack using deep convolutional neural network, International Journal of Pavement Engineering (2018) 1–7, https://doi.org/10.1080/10298436.2018.1485917.

[70] Z. Tong, J. Gao, Z. Han, Z. Wang, Recognition of asphalt pavement crack length using deep convolutional neural networks, Road Materials and Pavement Design 19 (2018) 1334–1349 2018/08/18 https://doi.org/10.1080/14680629.2017.1308265.

[71] K.E. An, S.W. Lee, S. Ryu, D. Seo, Detecting a pothole using deep convolutional neural network models for an adaptive shock observing in a vehicle driving, 2018 IEEE International Conference on Consumer Electronics (ICCE), 2018, pp. 1–2, , https://doi.org/10.1109/ICCE.2018.8326142.

[72] H. Gong, Y. Sun, Z. Mei, B. Huang, Improving accuracy of rutting prediction for mechanistic-empirical pavement design guide with deep neural networks, Constr. Build. Mater. 190 (2018) 710–718 2018/11/30/ https://doi.org/10.1016/j.conbuildmat.2018.09.087.

[73] Matwork, Statistics and machine learning toolbox user's guide, Matwork Inc., https://www.mathworks.com/help/pdf_doc/stats/stats.pdf, (2017) , Accessed date: 28 April 2018.

[74] M. H. Beale, M. T. Hagan, and H. B. Demuth, Deep Learning Toolbox User's Guide. Natick, MA 01760-2098: Mathworks, https://www.mathworks.com/help/pdf_doc/deeplearning/nnet_ug.pdf (Last Access Date: 05/11/2019), 2018.

[75] D.P. Kingma, J. Ba, Adam: A method for stochastic optimization, Proceedings of the 3rd International Conference on Learning Representations (ICLR), San Diego, vol. 2015, 2015.

[76] I. Goodfellow, Y. Bengio, A. Courville, Deep Learning, Adaptive Computation and Machine Learning Series, The MIT Press, 2016 ISBN-10: 0262035618.

[77] T. Whelen and P. Siqueira, "Coefficient of variation for use in crop area classification across multiple climates," Int. J. Appl. Earth Obs. Geoinf., vol. 67, pp. 114–122, 2018/05/01/ 2018, https://doi.org/10.1016/j.jag.2017.12.014.

[78] S. Sidney, Non-parametric Statistics for the Behavioral Sciences, McGraw-Hill, New York, 1988 ISBN 0070573573.

[79] A. Krizhevsky, I. Sutskever, and G. E. Hinton, "Imagenet classification with deep convolutional neural networks," Advances in Neural Information Processing Systems, https://papers.nips.cc/paper/4824-imagenet-classification-with-deep-convolutional-neural-networks.pdf (Last access date 05/11/2019), pp. 1097–1105, 2012.

[80] S. Dorafshan, R.J. Thomas, C. Coopmans, M. Maguire, Deep learning neural networks for sUAS-assisted structural inspections: Feasibility and application, 2018 International Conference on Unmanned Aircraft Systems (ICUAS), 2018, pp. 874–882, , https://doi.org/10.1109/ICUAS.2018.8453409.